



A-spiro: Towards continuous respiration monitoring

Justin Whitlock^{a,*}, Joshua Sill^b, Shubham Jain^{a,*}

^aDepartment of Computer Science, Old Dominion University, Norfolk, VA, United States

^bEastern Virginia Medical School, Norfolk, VA, United States

ARTICLE INFO

Keywords:

Breathing monitoring
 Continuous monitoring
 Respiration
 Chest band
 Wearable health sensing

ABSTRACT

This paper introduces A-spiro, a single-point wearable sensing technique to estimate respiratory flow and volume, in addition to respiratory rate. We show that when coupled with an inertial measurement unit, our system can accurately measure breathing parameters, even when the user is ambulatory. A-spiro can model lung hysteresis to separately predict increasing and decreasing trends of breathing flow. Existing techniques either monitor breathing rate only, or estimate volume and flow when the user is immobile, for example, sleeping. We validate our system for 20 users of different age, weight, height, and ethnicity, and capture breathing data across 6 different activities. For a total of 578 minutes of data, we show that A-spiro's generalized model for flow has an accuracy of 93% across 6 activities when compared to a spirometer. The estimated minute ventilation has an accuracy of 94.4%, while the estimated respiratory rate has a mean accuracy of 96% across all activities when compared to ground truth. We also compare A-spiro to a state-of-the-art system available commercially.

1. Introduction

Ubiquitous sensing technologies are increasingly being integrated into our daily routines in order to monitor our health and well-being. Tracking vitals, such as breathing and heart rate, can reveal information regarding a person's overall health, and plays an important role in health care. Breathing is a unique physiological phenomenon, both in healthy humans as well as those with respiratory disorders. In contrast to heart rate, breathing patterns are governed by both voluntary and involuntary input. According to the World Health Organization (WHO), more than 3 million people die each year from chronic obstructive pulmonary disease (COPD), which is estimated to be 6% of all deaths worldwide (World Health Organization, a). COPD is a class of diseases that cause limitations in the lung airflow, often diagnosed through a spirometry test. WHO strategies to curb the growth of preventable COPD include better surveillance and development of inexpensive methodologies for monitoring (World Health Organization, b).

Unmet Need. While continuous heart rate monitoring has found its way into our fitness trackers and smart watches, the optimal way to measure real-time variations in breathing is still largely an unsolved problem, albeit with potential for clinically significant impact. Mild perturbations in breathing patterns can be the first harbinger of early lung disease, often preceding the development of symptoms. Accurate lung function monitoring can have a significant impact on healthcare. Increased access to spirometry services has been shown to significantly benefit respiratory health and early diagnoses of respiratory illnesses (Jones et al., 2005). These services can also lower the cost of health care in under-served communities (Kumar et al., 2013) via tele-spirometry. Many children with chronic respiratory disorders such as cystic fibrosis are unable to verbalize respiratory symptoms or to cooperate with existing tests such as spirometry. A device which could measure minute ventilation in such patients, either in the home or during clinic appointments, could allow for earlier detection and treatment of respiratory distress. Such a system can not only monitor for early signs of pulmonary disorders, but also encourage users to improve their breathing technique under different circumstances.

*Corresponding author.

e-mail: jshcaffn@cs.odu.edu (Justin Whitlock), silljm@evms.edu (Joshua Sill), jain@cs.odu.edu (Shubham Jain)

Limitations of Existing Approaches. Despite their merits, the more recently proposed radio-based approaches have severe limitations. They only work where the required Wi-Fi infrastructure is present (Adib et al., 2015; Nguyen et al., 2016; Abdelnasser et al., 2015), which makes it very hard to use in outdoor environments. The bulk of the existing work (Adib et al., 2015; Fang et al., 2016; Abdelnasser et al., 2015) focuses on monitoring breathing rate alone, and does not estimate flow or volume. This is inadequate because voluntary control over the respiratory system allows significant variation in breathing patterns among individuals. A device that could also take into account the volume of ventilation over time would be a much more accurate predictor of respiratory function. Additionally, existing monitors only detect breathing parameters when the user is static - sitting or sleeping. This is a major limitation as they do not address scenarios where a user performs regular movements. Finally, these systems suffer from occlusion issues, and their performance varies based on the distance from the transmitter.

Challenges. Continuous respiratory monitoring is highly desirable but extremely challenging. Unlike heart rate, breathing signals do not have a predictable pattern of repetition. Breathing cycle lengths and the size of each breath can vary significantly from one breath to another. This renders traditional frequency domain measurements ineffective. Moreover, sensor measurements of user's chest wall movement are corrupted by noise, such as the user's body movement. This makes it difficult to extract breathing patterns from ambulatory users. Simple acts such as moving one's limbs or transitioning from standing to sitting can affect the sensor measurements.

Proposed Approach. We present A-spiro, which addresses these challenges by introducing a low-cost, unobtrusive sensing system that continuously monitors a user's respiratory parameters - respiratory flow, minute ventilation, and breathing rate. Our system name is derived from *aspiro* which means to breathe, in Latin. The A-spiro prototype consists of a wearable sensor that is integrated into a belt worn around the chest (Figure 2). What distinguishes A-spiro from existing approaches is that A-spiro works accurately even when the user is in motion (non-static). In summary, A-spiro makes the following contributions:

- A-spiro is the first wearable system that provides accurate estimates for breathing flow and minute ventilation using single-point sensing
- A-spiro incorporates techniques for motion correction to provide accurate estimates even when the user is non-static. We present the design and development of algorithms for breathing signal extraction from noisy chest movement data.
- A-spiro is validated for 20 users in 34 individual sessions. Our total breathing data amounts to 190 3-minute traces across 6 activities.

2. Breathing Primer

Mechanics of breathing. The most important muscle during breathing is the diaphragm, which is a dome-shaped muscle near the lower ribs. Inspiration, or inhalation, occurs when the diaphragm contracts, forcing the abdominal contents down and the chest cavity is increased. Normal breathing is also known as tidal breathing. The amount of air a person inhales during a normal breath is called tidal volume (V_T). In normal tidal breathing, the distance moved by the diaphragm is small. In contrast, expiration is passive during tidal breathing. The lungs and chest wall are elastic and have a natural tendency to return to their initial resting position after an inhale.

Measuring lung volume. Respiratory rate alone is not indicative of lung conditions. Standard lung function tests, such as spirometry, measure change in lung volume over a small duration as one breathes. In a spirometry test, one breathes into a mouthpiece that is connected to an instrument called a spirometer (Nuffield Foundation), that measures airflow. It is a valuable investigation in the management of patients with suspected or previously diagnosed respiratory disease, such as asthma, COPD, or cystic fibrosis.

Spirometry. The most common method for measuring lung function is through the use of a spirometer (Nuffield Foundation; Cleveland Clinic). There are two categories of spirometers (Parreira et al., 2005). Flow oriented spirometers measure the amount of air passing through a tube over a certain amount of time. Measurements are typically given in liters/second. Volume oriented spirometers measure displacement in liters. Spirometry tests are given in a clinic, with the goal of determining healthy lung function during a maximal respiratory effort. Spirometry is an intrusive process, that requires the users to breathe into a mouth-piece, while their nose is closed with a clip.

Breathing parameters. Spirometry results include respiratory rate (RR), tidal volume (V_T), and minute ventilation (V_M), among many others. RR is typically given in breaths/minute. The measurement is derived from 10 or 15 secs of normal breathing. V_T is the average volume inhaled or exhaled during a single cycle of normal breathing, also called tidal breathing. V_M is the total volume of air passed through the lungs within a minute. Like RR , the V_M measurement is derived from 10 to 15 seconds of breathing (Cleveland Clinic).

3. System Design and Overview

Our primary idea is to monitor respiratory parameters for static as well as non-static users. A-spiro considers two primary causes for chest movement: first is that caused by larger body movements, such as limb movement, sitting, standing, walking, etc; second, the minute chest wall movement caused by breathing. For the rest of this paper, these motions are referred to as body motion and breathing motion, respectively. Breathing motion is more notable when the user is static. Past work (Liu et al., 2015; Abdelnasser et al., 2015; Nguyen et al., 2016; Liu et al., 2016; Fang et al., 2016) has leveraged this fact to detect breathing rate when the user is sitting, standing still, watching TV, or sleeping. A-spiro aims to eliminate this primary assumption of the user being static for breathing detection.

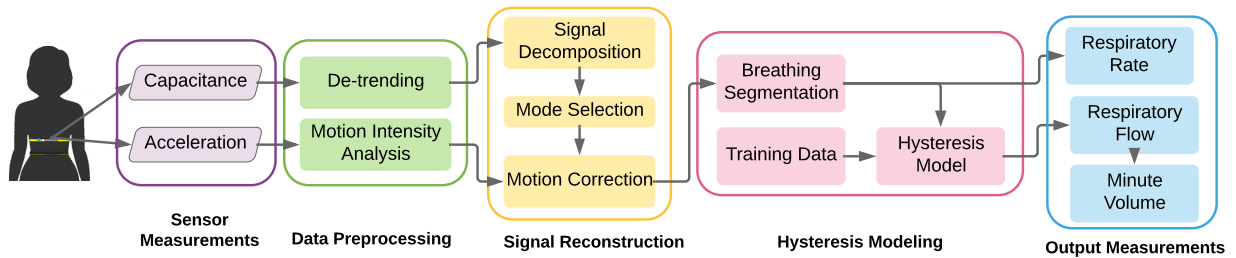


Fig. 1: A-spiro: System Overview.

3.1. Challenges

Real-time accurate monitoring of respiratory parameters is non-trivial, primarily for three reasons. First, despite the overwhelming amount of breathing monitoring systems, the fundamental bottleneck is user motion. Existing systems are highly susceptible to user motion (Fang et al., 2016; Nguyen et al., 2016; Abdelnasser et al., 2015). Any breathing signal obtained when the user is moving is corrupted and is often discarded (Adib et al., 2015). Chest movement caused by breathing is significantly smaller than that caused by body motion. Any breathing signal obtained when the user is moving is lower than the noise floor, and its extraction is non-trivial. Lack of tools to monitor breathing for a mobile user has significantly limited its applications to events where a user is quasi-static, such as sleeping. Second, monitoring breathing volume is more complicated than computing respiratory rate, and often requires intrusive means. This is primarily due to the non-linear relationship between breathing volume and chest movements. Third, continuous monitoring via wearable systems is limited due to the inconvenience of wearing multiple sensors on different locations of the body, including but not limited to a chest belt, abdomen belt, and a nasal probe (NOX Medical).

3.2. Design Goals

In lieu of the above challenges and limitations of existing systems, we propose the following design goals:

- **Minimal single-point non-intrusive sensing.** To address the challenge of multiple point sensing - involving multiple sensors that a user is required to wear on different body locations- we propose a single-point non-intrusive sensing solution. Our goal is to only gather data from a single point on the human body to compute the required breathing parameters.
- **Monitoring respiratory flow and volume.** Past research has focused on monitoring the number of breaths per minute, i.e. the breathing rate. Although important, the breathing rate is inadequate in determining more critical changes in a person's breathing - such as the depth of each breath. This depth is represented by the volume of air that moves through a person's lungs during inhalation and exhalation. A finer parameter, the rate of flow of the air into and out of the lungs can aid in deducing difficulties in breathing and obstruction. Thus, in addition to breathing rate, the system should be able to measure flow and volume.
- **Continuous monitoring for non-static users.** A major goal of our system is to measure breathing even when the user is ambulatory and performing activities of daily living. Our sample activities include walking, carrying and setting things down, transitioning between sitting and standing, sitting, standing, and meditating. Continuous monitoring of breathing will have a significant impact, particularly for those who might be unable to express difficulty in breathing, such as children and the elderly.

3.3. Overview

The system design for A-spiro is illustrated in Figure 1. It consists of a strain or stretch measurement sensor that measures expansion and contraction on the sensor. Our goal is to measure two variables: breathing motion and body motion. As we only use a stretch sensor that measures along a single dimension, the problem is underconstrained. To address this, we add an inertial measurement unit (IMU) to our prototype. These sensors are worn around the chest as part of a belt as shown in Figure 2, and continuously transmit stretch, accelerometer, and gyroscope measurements over a Bluetooth channel. We use a non-stretchable belt for our prototype as it allows for easy access and wearability. A-spiro's sensors do not need to be in contact with the skin, and thus the belt can be worn over regular clothing. In the future, the combined sensing system can be integrated in clothing, such as hospital gowns or undershirts.

A-spiro's sensor data processing pipeline consists of three building blocks. At the input, the raw sensor measurements are provided to the *Data preprocessing* module. The raw readings are the capacitance measurements from the stretch sensor and accelerometer data from the IMU. When the stretch sensor expands or contracts, the output capacitance measurements from the sensor vary linearly. We prove that the capacitance measurements are linear with respect to the stretch distance, in Section 6.4. These sensor streams are processed to de-trend the capacitance readings by analyzing instantaneous change only. The

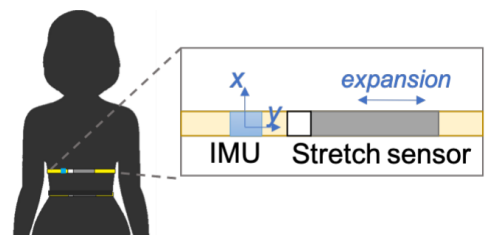


Fig. 2: The A-spiro sensing unit is positioned at the xiphoid, at the bottom of the breast bone. It consists of a stretch sensor and an IMU. It is worn over regular shirt, or can be integrated into a close fitting shirt.

accelerometer data is processed to determine user’s motion intensity and identify periods of motion. The goal of this module is to prepare the data for the breathing signal to be extracted.

The *Breathing signal reconstruction* module decomposes the signal across a time-frequency scale. Breathing does not occur at regular intervals, and due to the variation in frequency over time, Fourier analysis proves insufficient. Instead, we employ empirical mode analysis to decompose the signal into various modes, that are then selectively combined to generate the filtered output. A-spiro then performs motion correction based on the body motion intensity, as detected by the IMU analysis. Finally, the *Hysteresis modeling and flow estimation* module segments breathing data based on lung hysteresis to learn a model that can predict respiratory flow from filtered capacitance, or stretch measurements. We integrate the model response to obtain the minute ventilation.

4. A-spiro Processing Pipeline

In this section we present the details of A-spiro’s processing pipeline shown in Figure 1.

4.1. Preprocessing

We preprocess the sensor data before extracting breathing signal from it.

4.1.1. Noise Removal

The breathing process generating the signal obtained from the stretch sensor is non-stationary and non-linear. An example of the raw data obtained is shown in Figure 3. Figure 3a shows the capacitance readings obtained from a single participant during sitting. These capacitance readings are indicative of the chest expansion and contraction. Raw sensor data for transitioning from sitting to standing and vice versa a few times, is shown in Figure 3b and that for walking is shown in Figure 3c. We can observe that the stretch values lie in a different range for each individual and activity because the sensor value initializes at different capacitance every time it is worn, depending on the circumference of a person’s chest and the mounting differences. To remove the offset arising from variations in body size and mounting, rather than looking at raw stretch values, we consider the instantaneous change only by calculating the first order differential of the sensor data. Taking the differential of the stretch values also has the advantage of being a similar metric to the breathing flow (measured in L/s) values obtained from the spirometer, which is our target for prediction. The resulting signal is de-trended but contains a great deal of noise, and is filtered during signal reconstruction.

4.1.2. Motion intensity detection

During periods of body motion, chest movement corrupts the breathing signal obtained from the capacitive sensor. Unlike other systems (Nguyen et al., 2016; Adib et al., 2015; Fang et al., 2016), instead of discarding breathing traces corrupted by motion, we use feedback from the IMU to reconstruct the degenerate segment of the signal. The goal of the preprocessing step is to use the accelerometer to determine the level of activity intensity as the variance of the accelerometer data. Sitting, standing, and meditation exhibit very low variance compared to activities that involve movement of large body parts, such as limbs, or twisting of the upper body.

4.2. Breathing Signal Reconstruction

At the onset, it may seem that body motion and breathing motion can be separated using frequency domain analysis, such as Fourier transform. We present why Fourier analysis is not ideal for our purpose and the techniques employed thereon.

4.2.1. Limitations of Fourier Analysis

Traditionally, signal separation has been performed by transforming a time-series signal to the frequency domain. However, this is effective only when the signal is stationary. Breathing signal is non-stationary. Note that this is not a factor when calculating respiratory rate since it only counts the number of cycles. Fourier analysis assumes stationarity and decomposes a signal into sinusoidal waves. However, breathing waveforms exhibit time-varying frequencies, thus affecting the density of frequency components in the captured signals. Figure 4 shows the power spectrum analysis for two different activities: sitting and walking, and the corresponding band pass filtered signal at the frequency component with the highest power (Figure 4b and 4c). For A-spiro the change in stretch is inversely proportional to the flow. We can see that when the participant is sitting, the correlation between stretch measurements and breathing flow is somewhat consistent, but the amplitudes are severely suppressed for deep breaths- those with higher amplitude than regular breathing. For walking, the resultant signal has many frequency components, and using a single frequency for signal separation yields a somewhat flat trace that does not capture the person’s breathing well. Thus, Fourier analysis is not ideal when the user is moving and performing tasks that have multiple frequency components.

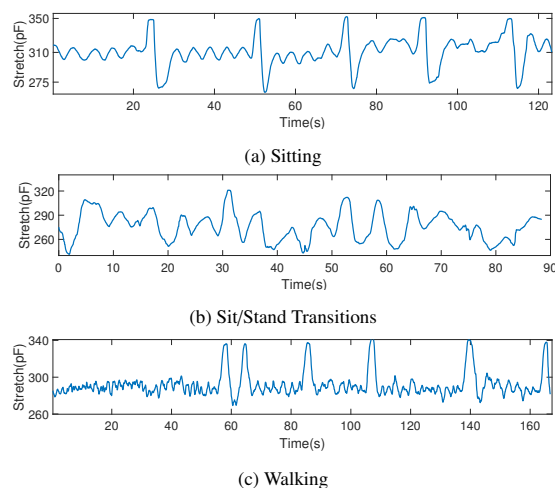


Fig. 3: Raw signal from the stretch sensor for 3 activities: sitting, transitioning between sitting and standing, and walking on a treadmill. (a) Higher amplitude sections during sitting denote deep breaths. Breathing signal is corrupted by body movements (b) and (c).

4.2.2. Extracting breathing signal

To overcome the challenges posed by Fourier analysis and similar techniques, we use part of the Hilbert-Huang Transform (HHT) (Huang et al., 1998), which aids in analyzing non-linear non-stationary signals. This crucial processing part of the HHT is Empirical Mode Decomposition (EMD). EMD is a data-driven approach that performs adaptive time-space analysis for signals, and does not make any assumptions about the underlying nature of the signal. Using EMD, we decompose our signal into finite and small number of single oscillatory modes called intrinsic mode functions (IMF). EMD considers a signal at the level of local oscillations. A given stretch signal $s(t)$ is decomposed as:

$$s(t) = r(t) + \sum_{k=1}^K d_k(t) \quad (1)$$

where $r(t)$ is the residual trend and $d_k(t)$, $k = 1, 2, \dots, K$ denote the modes. The modes and the trend are both constrained to be zero-mean amplitude-modulated frequency-modulated (AM-FM) waveforms. EMD identifies these modes through a sifting process. Our implementation of EMD follows the HHT. In each iteration, we determine the local maxima $s(t)_{max}$ and local minima $s(t)_{min}$ of the signal $s(t)$. Its upper and lower envelopes are determined from a cubic-spline interpolation of local maxima and minima. If $\mu_1(t)$ is the mean of its upper and lower envelopes, the first component of $s(t)$ is given by:

$$d_1(t) = s(t) - \mu_1(t) \quad (2)$$

In the second iteration of the sifting process, $\mu_1(t)$ is treated as the data and the process is repeated to obtain $\mu_{11}(t)$, which is the mean of $d_1(t)$'s upper and lower envelopes. The second iteration yields the second component $d_2(t) = h_1(t) - \mu_{11}(t)$. The sifting process is repeated k times, resulting in a set of finite functions, the number of which depends on the original signal.

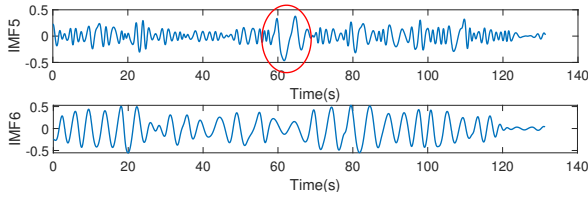


Fig. 5: Mode mixing: The signal has been separated into IMF 6, but a single breathing cycle has been pulled into the previous IMF.

However, EMD suffers from mode mixing for our data. The ratio of the amplitudes and of the frequencies of the individual components of the signal, determine whether EMD will be able to separate them in two different IMFs or whether they will be interpreted as one single IMF. When a mode cannot clearly contribute with extremas, the EMD will not be able to separate the mode in a single IMF and the mode will remain mixed in another IMF. An example of mode mixing from our data is shown in Figure 5. This mode mixing is more prominent when noise due to motion or other factors temporarily impact the signal or drop out of the signal, resulting in part of the signal appearing in a different IMF than expected. To address the challenge of mode mixing, we implement an advanced version of EMD, known as Ensemble Empirical Mode Decomposition (EEMD) (Colominas et al., 2014).

EEMD is a noise-assisted analysis technique. Instead of sifting through the raw signal as EMD does, EEMD sifts through an ensemble of white noise-added signal. We add a gaussian white noise signal to our input data, with a standard deviation that is one-fifth that of the input signal. The addition of white noise ensures that the ensemble exhausts all possible solutions in the sifting process. Due to the time-space analysis, the added finite white noise is averaged out with sufficient number of trials. EEMD is built upon EMD. It utilizes the scale separation capability of EMD and enables it to be a dyadic filter bank. By construction, each IMF is a zero-mean waveform whose number of zero-crossings differs at most by one from the number of its extrema. The number of these zero-crossings is a rough indication of the mean frequency of each mode, and the way this number varies from mode to mode is an indication of the hierarchical structure of a filter bank.

4.2.3. Mode selection

From the results of the signal decomposition, the IMFs are evaluated for trend-stationarity. It has been shown that stationarity can be an important metric for evaluating individual IMFs (Terrien et al., 2011). In general, a signal is said to be stationary only if its statistical moments

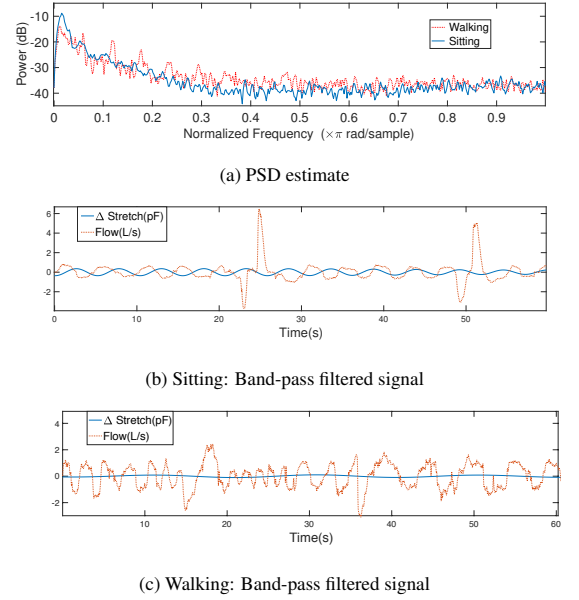


Fig. 4: (a) Power spectrum analysis for sitting and walking traces. Note that walking has many more frequency components (peaks). (b) The corresponding band pass filtered signal for sitting and (c) walking, compared to the ground truth. Fine grained shifts in breathing rate and depth are not captured. Deep breaths are not captured.

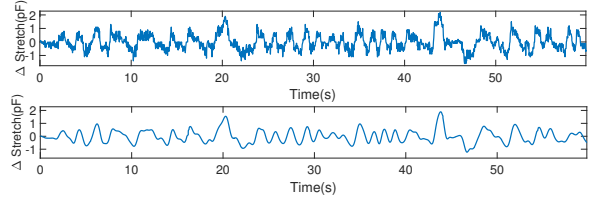


Fig. 6: The top figure shows the signal before EEMD filtering. The filtered signal below is obtained after mode selection.

are constant over time. However, a weak-stationarity can be established for some biological signals using a Kwiatkowski-Phillips-Schmidt-Shin (KPSS) test (El-Tatar & Fokapu, 2011). The KPSS algorithm assumes a time signal is composed of its deterministic trend, random walk, and the stationary error.

$$s(t) = \beta t + \mu_t + \epsilon_t \quad (3)$$

Where β is the deterministic trend, μ_t is the random walk, and ϵ_t is the stationary error. Under the null hypothesis, the variance $\sigma_\mu = 0$, implying the random walk acts as a constant. When the deterministic trend $\beta = 0$, as it is for our signal, KPSS can be used to establish weak stationarity of a signal (El-Tatar & Fokapu, 2011). For our purposes, the first 2 IMFs in the series were observed to be high-frequency noise and were skipped. IMFs 3 to K were evaluated consecutively using KPSS. The first positive result, I, indicates the beginning of the breathing signal. The reconstructed signal in Figure 6 is then obtained by adding I to K IMFs, including the residual.

$$f(t) = r(t) + \sum_{k=I}^K d_k(t) \quad (4)$$

An example for an input signal and the corresponding filtered output is shown in Figure 6.

4.2.4. Motion correction

To maintain an estimate of the user's breathing parameters even during body motion, we propose a motion correction technique that utilizes feedback control. A-spiro uses this feature to create a motion cover, m . m is set to high when the motion intensity detection indicates body motion. The inherent property of a breathing signal is the occurrence of cycles. Although the frequency and duration of individual breaths may vary over time and across activities, a breathing signal always has alternate polarity - positive or negative - signifying the in-hales and ex-hales. A-spiro's motion correction is triggered when the state of m is high, and the breathing signal obtained during that interval is considered to be corrupted. For low-impact low-intensity body motion, we observed that only a single breathing cycle was corrupted by each body motion event. One of two phenomena can be observed when body motion occurs. On a negative-going cycle, for example, a sudden motion could either reverse the polarity of the observed signal or slightly modify the amplitude of that cycle. This is usually followed by high frequency-noise. The breathing signal extraction explained in Section 4.2.2 takes care of the high frequency noise, which leaves the corrupted cycles to be corrected for motion. A-spiro analyzes the polarity of the breathing cycles immediately preceding and following the time period t_m , where $m = 1$. Based on the polarity of these cycles, A-spiro predicts the polarity for the waveform during t_m . If the observed polarity matches the predicted polarity, A-spiro retains it. If the observed polarity does not match the predicted polarity, A-spiro reverses the captured signal, as depicted via a sample in Figure 7. A positive polarity cycle was flipped when motion started. A-spiro identifies the negative cycles before and after the motion affected cycle, and reversed it around the x-axis. This trace was collected during transitions from sitting to standing, and all motion-based corrections were verified against the ground truth. We compare our breathing signal capture efficiency with the baseline approach of discarding segments with motion. Figure 8 plots the amount of signal captured by A-spiro after motion correction and the signal captured if the segments with motion were discarded. These numbers were computed across all the participants for all activities. We can see that even during simple activities, such as sitting and standing, up to 15% of breathing signal can be lost due to motion. A-spiro corrects these segments to increase the amount of captured breathing signal up to 100%. For activities with small aperiodic body movements, A-spiro captures more than 95% of the breathing signal, compared to 80% capture by the baseline approach. For activities involving repetitive periodic movement, such as walking, the baseline approach only captures 30% of the breathing signal, while the rest is lost due to body motion. A-spiro, on the other hand, captured 100% of the breathing signal despite large body movements.

4.2.5. Isolating breathing cycles

Breathing cycles are isolated by first finding the zero-crossings of the zero-mean filtered signal obtained after reconstruction and motion correction. The zero-crossings are then evaluated to determine a transition between inhale-exhale (negative polarity) or exhale-inhale (positive polarity), based on three criteria. The thresholds for various criteria are guided by general practices in spirometry and our own observations. The first measures the interval between the current zero-crossing, and the next zero-crossing in time. If the interval is too short, less than 0.5 s, the second crossing is discarded, and the new interval is considered to be part of the current cycle. The second criterion determines whether the polarity for the current interval is opposite in sign to that of the next interval, indicating that the next zero-crossing defines a change from inhale or exhale. If not, the next zero-crossing is discarded, and the cycles are considered the same. The third criterion takes the integral of the interval data. The integral for a cycle denotes the volume in that cycle. If the integral is below a threshold of 0.2 pF^2 , the zero-crossing is discarded. In the resulting set of zero-crossings, every alternate crossing represents the start of a new breathing cycle.

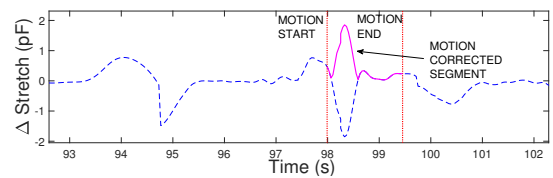


Fig. 7: Example for motion correction during sit/stand transition. The red lines indicate the start and stop of motion detected by the accelerometer. The captured blue dashed trace is corrected to a positive cycle, shown in solid magenta.

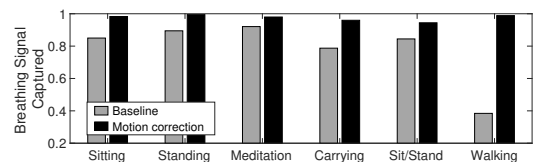


Fig. 8: Breathing signal captured by using the proposed motion correction technique versus baseline approach of discarding motion segments.

4.3. Breathing Parameter Estimation

In the final stage of A-spiro, we model the stretch measurements to predict breathing flow.

4.3.1. Hysteresis Modeling.

One of the critical characteristics we address in our system design is that of lung hysteresis. The lung is an imperfect elastic body and hence dissipates energy. The energy consumed by the lung in inspiration is not recovered in expiration. This causes a delay in response to changes in chest wall movement by the lungs, and vice versa. Simply put, this implies that the distribution of chest wall motion will not be identical during inhalation and exhalation, or the ascending and descending directions of chest expansion, showing hysteresis. Figure 9 annotates the inhales and exhales on a filtered stretch signal. The inhales are the positive cycles, and exhales are the negative cycles. A positive trend denotes transition from exhale to inhale, while a negative trend denotes the opposite direction. Hysteresis states that the positive and negative trends will be unlike. Therefore, contrary to existing approaches where breathing signal is split into inhales and exhales, we split them by trend: positive and negative. This impresses the need for segmenting the sensor output in real-time and monitoring trends in rate of change separately. As outlined in Algorithm 1, we train separate models for each trend using a fourth-order Fourier series. Depending on the trend, the relationship with the ground truth flow follows different paths, as seen in Figure 10. This fine-grained signal segmentation and targeted data modeling allows us to account for hysteresis more accurately. Figure 11 shows the output from the hysteresis model compared to the flow from the spirometer. We can see that the estimated flow closely matches the actual flow trace obtained from the spirometer. We perform a quantitative evaluation in Section 6.

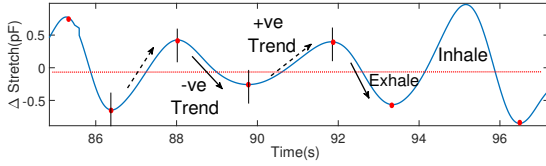


Fig. 9: The positive cycles indicate inhales; the negative cycles indicate exhales. Trends in stretch, are marked by the arrows. Positive trend denotes transition from exhale to inhale; negative trend indicates transition from inhale to exhale.

4.3.2. Estimating Breathing Rate, Flow, and Volume.

The respiratory rate is calculated after isolating the breathing cycles (Section 4.2.5). Once small spurious cycles have been consolidated into larger inhale and exhale cycles, we count the number of breaths per minute to obtain the respiratory rate, RR . The model described in Section 4.3.1 predicts the flow when provided stretch measurements as input. Breathing flow denotes the rate of change of volume expired or inspired. According to our ground truth spirometer, positive flow indicates exhales and negative flow indicates inhales. Minute ventilation, V_M is the amount of air inspired (or expired) during normal breathing in one minute. Minute ventilation increases with activity to accommodate increased need for gas exchange. We calculate V_M from flow by integrating the inhales and computing the volume for one-minute duration.

$$V_M = \int_{in} F dt \quad (5)$$

We evaluate A-spiro's accuracy in estimating RR and V_M across all subjects and activities.

```

Data: FilteredData
Result: Predicted_Flow, RR, VM
(+veModel, -veModel) ← initialize
for window in FilteredData do
  RR ← calcRR(window)
  (+veTrend, -veTrend) ← split(window)
  incr_Predict ← +veModel(+veTrend)
  decr_Predict ← -veModel(-veTrend)
  Predicted_Flow ←
    reconstructWindow(incr_Predict, decr_Predict)
  VM ← calcVM(Predicted_Flow)
end

```

Algorithm 1: Breathing parameter estimation from stretch signal.

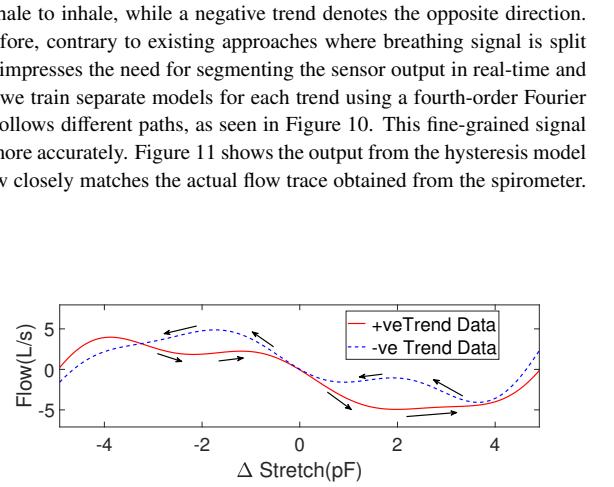


Fig. 10: Hysteresis: The rate of change in chest circumference shows a non-linear correlation with air flow, and follows a different path depending on the direction of change.

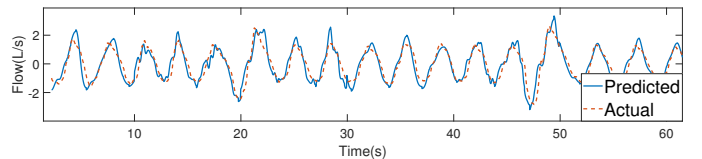


Fig. 11: The predicted values from the hysteresis model compared to the ground truth from the spirometer while the volunteer was standing.

5. Experiment Description

Prototype. We chose a capacitive strain sensor from Stretch Sense (Stretch Sense). The sensor is Bluetooth ready, with a stretchable fabric sensing surface as shown in Figure 12. The sensor was sewn to a velcro strap to allow an adjustable fit. For the strap, materials with any elasticity were avoided to ensure all motion of the chest wall is captured by the sensor and not lost due to stretching of the strap. The velcro backing on the strap also clings to the fabric of the users clothing, preventing the sensor from slipping during body movement. The sensor is 10 cm long and can stretch comfortably to 18 cm. An inertial measurement unit (IMU) was attached to the belt, next to the stretch sensor. We logged the accelerometer data from the IMU over Bluetooth. Both, the capacitance sensor and the IMU were sampled at 30Hz. While the sensors are attached to a belt for the prototype, in the future they can be integrated into clothing, particularly due to the fabric construction of the stretch sensor.

Position. We tested the sensor in several positions; the abdomen, the back, the side, upper chest, and the xiphoid, which is the center of the chest over the lower part of the breast bone, as seen in Figure 2. The xiphoid was chosen since the breast bone is easy to locate. This ensures that the sensor was positioned consistently between subjects and tests. It would also be easier to implement in a real life context such as self-care, compared to a position like the center of the back.

Participants. We recruited 20 volunteers for our study, of which 11 were male and 9 female. Lung volume is affected by demographics and personal information, such as age, weight, height, and ethnicity. To account for the diversity we recruited participants from a large variety of age and ethnic groups. Of the 20 participants, 2 were undergraduate students, 5 graduate students, and the rest were working professionals. Details on our study population are provided in Table 1. To validate the feasibility of our system, we recruited healthy adults for our study, those that do not exhibit any breathing disorder.

Ethnicity	# subjects	Age Group	# subjects
Caucasian	12	18-20	2
African	2	20-30	4
Hispanic	2	30-40	7
Asian	2	40-50	5
Other	2	50-60	1
		60-70	1

Table 1: Participant Demographics

Data Collection. We collected data for 6 different activities. 3 of these activities involved the user being stationary, while the other three engaged them in Activities of Daily Living (ADL). The experiments were conducted in 2 sessions on separate days, where the participant performed all six activities in each session. Our goal in the selection of these activities is to mimic real-world scenarios as far as possible. Each activity lasts up to 3 minutes. Among the stationary, or static, activities, the first was *sitting*, wherein users sat on a chair as shown in Figure 13a. Volunteers were asked to read from a screen, so that they were distracted from consciously affecting their breathing, capturing the range of flow for tidal breathing. The second activity was *guided meditation*. During this activity, we played a guided meditation video (Chopra, 2018) allowing the users to be mindful of their breathing and taking slow deep breaths. The third activity was *standing*.

To understand how performing an activity affects the data, we had volunteers perform a number of tasks to reflect daily life activities. In this set of activities, the first was *transitioning from sitting to standing and back to sitting* (referred to as *Sit/stand*). During this activity, we asked the user to start either in the seated or standing position, and transition to standing (or sitting). They were asked to do this a few times during three minutes, where they were free to choose when to perform the transition. The second activity involving motion, required volunteers to *pick up a book from one table, turn around and set it on another table* (referred to as *Carrying*). This introduced a twisting motion to the torso. Finally, our volunteers were asked to *walk on a treadmill*, shown in Figure 13b, at a self determined comfortable pace, no faster than 3 mph.

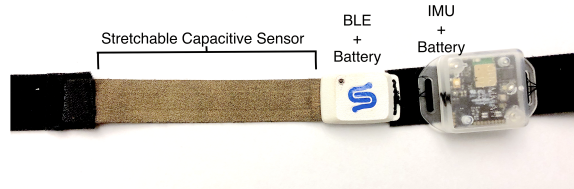


Fig. 12: A-spiro prototype. Stretch sensor and IMU attached to Velcro strap.



(a) Sitting in lab.

(b) Walking on treadmill.

Fig. 13: Data collection setup. The participants wore the A-spiro wearable while breathing into a spirometer (used for ground truth).

6. Evaluation

A-spiro measures three key breathing parameters: respiratory rate (RR), tidal flow, and minute ventilation (V_M). We evaluate A-spiro with respect to the flow data output from the NDD spirometer (New Diagnostic Design).

6.1. Respiratory rate

The respiratory rate is measured in breaths per minute (bpm). Figure 14 shows the median accuracy across all participants for each activity. We can see that for all the activities, our median accuracy is higher than 90%. While the accuracy is higher than 95% for static scenarios, A-spiro achieves greater than 90% activity even when the subjects were walking, transitioning between sitting and standing, and carrying a book.

6.2. Breathing flow estimation

To evaluate the time-series flow estimates predicted by our model, we use the flow measurements from the Spirometer as ground truth. We measure the normalized root mean square error, given by:

$$NRMSE = \sqrt{\frac{\text{mean}(\hat{f}_t - f_t)^2}{f_{\max} - f_{\min}}} \quad (6)$$

where \hat{f}_t is the predicted flow measurement and f_t is the observed measurement (from the spirometer). We also define the accuracy of our system as $Acc = 1 - NRMSE$.

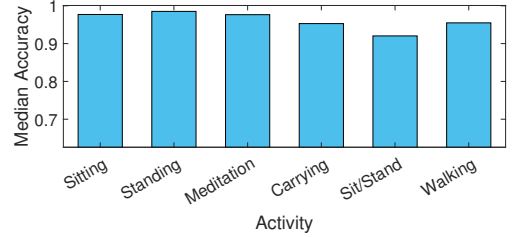
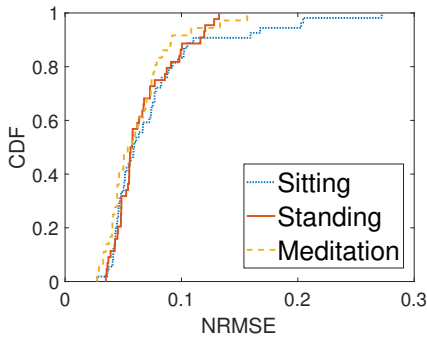
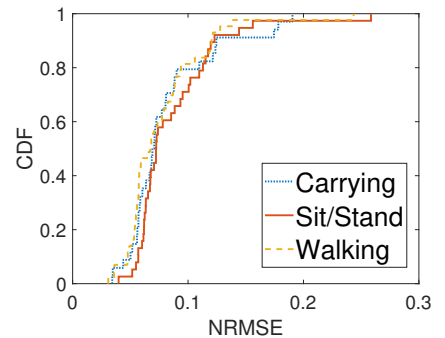


Fig. 14: Respiratory rate accuracy across all traces for different activities.



(a) Static Activities



(b) Non-Static Activities

Fig. 15: Leave-one-out cross-validation for a generalizable model for flow estimation. Models were trained on $N-1$ volunteers, and tested on the remaining volunteer.

We report the results of flow measurement across all participants using leave-one-out (LOO) cross-validation technique. Our goal here is to analyze how generalizable capacitance-flow models are. For each run, we use $N - 1$ participants for training the hysteresis model and test it on the one participant left out. Thus, at each time, our training data comprises of data from 19 participants. We compute the $NRMSE$ 20 times for each activity and plot the CDF. Figure 15a shows the normalized RMSE for the three static activities where the user is not moving: sitting, standing, and meditating. We see that the performance for all these activities are quite similar, due to the absence of motion in all cases. The median error is approximately 7%. This translates to a significant improvement over the state-of-the-art that requires separate learning models for each participant and added infrastructure, with similar performance, adding to overall time and cost of the system.

Figure 15b plots the error for non-static activities: carrying a book and setting it down, transition between sitting and standing, and walking. Despite varying intensities of motion, we see that the median for all three non-static activities is approximately 8%, indicating the accuracy of the motion correction algorithm. This shows that our hysteresis model accurately models changes in chest expansion to changes in lung flow for both static and non-static scenarios. In a different validation, we build personal models for each participant and test them against all other participants, one at a time. Figure 16a shows the confusion matrix for static activities and Figure 16b shows the confusion matrix for non-static activities. The participants are sorted in the order of Body-Mass Index (BMI). It is known that lung flow and volume depend on many characteristics, including age, weight, height, and ethnicity. We choose BMI as a parameter to validate how well a model trained on one person tests against other participants with similar or different BMIs. It is expected that people with similar BMI will exhibit higher correlation, and the confusion matrix will be a diagonal matrix with a certain deviation. On careful examination we can see that to be true. However, we also witness other examples where models trained on certain participants are more generalizable against a large population of the participants.

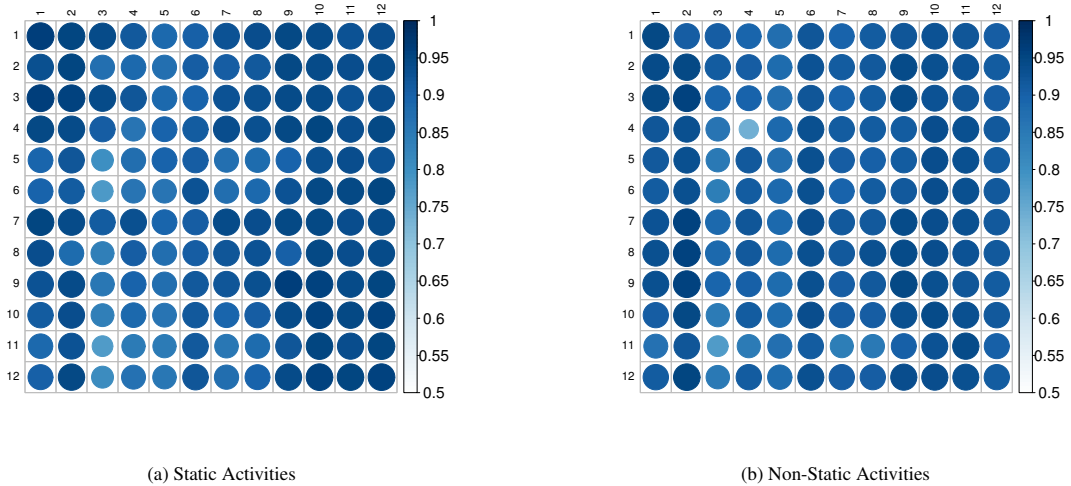


Fig. 16: Confusion matrix for personal flow estimation models across participants. Y-axis represents data used for training; X-axis represents data used for testing. Models are validated on (a) static activities (sitting, standing, and meditation), and (b) non-static activities (sit/stand, carrying, and walking).

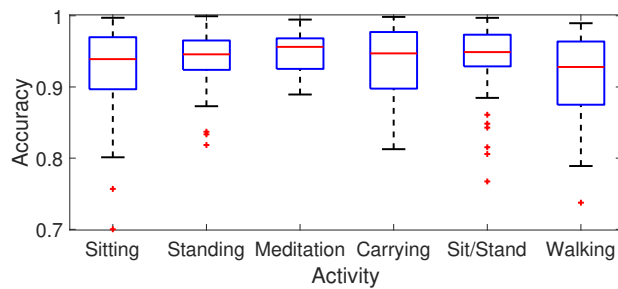


Fig. 17: Minute ventilation accuracy across different activities.

6.3. Minute Ventilation Estimation

We integrate the flow measurements for inhale and exhale cycles to compute the volume during each phase. We then compute the minute ventilation by analyzing the exhale volumes for separate dis-joint one-minute windows, and compute the V_M for each trace by taking a mean. Minute ventilation accuracy for all participants across different activities is shown in Figure 17. This accuracy was calculated using leave-one-out validation, as described for tidal flow estimation. We can see that the median accuracy for all activities is higher than 90%. We observed that sitting exhibits large deviation due to small shifting movements, leaning backward/forward, and sometimes slouching during the sitting duration. Of all our activities, sit/stand transitions show the most variance, due to the sudden large body movements.

6.4. Sensor repeatability and accuracy

Continuous monitoring of breathing is fundamentally dependent on the accuracy and precision of the sensor being used. The output capacitance of the stretch sensor changes as the sensor is stretched. Repeatability requires that, for the same stretch, the sensor should undergo the same change in capacitance. To validate this we performed a test where we stretched the sensor through distances of 10 cm - 16 cm in steps of 2 cm, and recorded the capacitance each time. Figure 18 displays the change in capacitance with change in stretch distance. We can see that over 20 trials, the variation of capacitance is extremely small. Our mean coefficient of variation was 0.0032. These tests were conducted on separate non-consecutive days. In fact, capacitance and stretch measurements are seen to have a positive linear correlation, with a Pearson correlation coefficient of 0.998. We use these

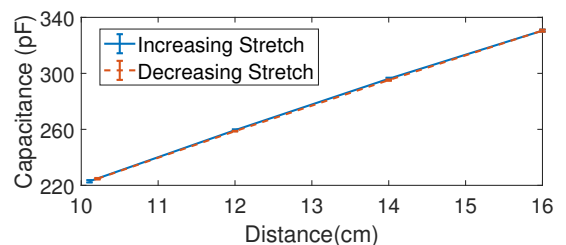


Fig. 18: The relationship between distance of stretch and capacitance output by the sensor is linear.

readings to build a linear regression model which yields the stretch given a capacitance measure. The root mean squared error for this model was 0.09. This demonstrates that the stretch sensor provides repeatable measurements. We also validated the sensor measurements when it was worn by the user. To record the ground truth for chest expansion measurements, we attached a measuring tape to the chest strap, that moved as the sensor stretched. When a person sits and breathes, we recorded a video and manually observed the change in the measuring tape readings, which served as the ground truth. We use the linear model discussed above to compute stretch measurements corresponding to capacitance values. We observed a variation of only $\pm 0.3\text{cm}$ from the ground truth. This demonstrates that the stretch sensor provides accurate and repeatable measurements, when mounted on the chest.

6.5. Comparison with HexoSkin Smart Garment

We compare A-spiro with a commercially available state-of-the-art health tracking system, HexoSkin (Phillips et al., 2017). HexoSkin is designed to continuously track RR , V_M , and V_T , as well as other non-breathing related metrics like heart rate. It captures the breathing signal using two inductance bands where the sensor entirely encircles the torso at the chest and abdomen for men, and the abdomen only for women. The sensors are embedded within a smart garment, and users are asked to input age, height and weight in order to accurately estimate health metrics. It has also been shown that movement can disturb the vest’s ability to accurately measure breathing (van Leuteren et al., 2017). We used raw data from a flow based spirometer as the gold standard for respiration monitoring, to perform a side by side comparison with A-spiro and Hexoskin. For each device, we computed the relative error of the estimated respiratory rate with respect to the value obtained from the spirometer. V_M is estimated from flow by calculating the exhaled volume using equation 5 during each non-overlapping period of one minute and taking the mean over all one-minute intervals. We compared the two systems for sitting and walking for 3 participants. The participants were male, and of similar height and weight. For each participant, we recorded 4 traces, amounting to a total of 36 minutes of data. As shown in Figure 19, A-spiro significantly improves upon the performance of Hexoskin for both activities. While A-spiro is impacted by motion, the impact is considerably lessened as compared to Hexoskin, particularly for V_M .

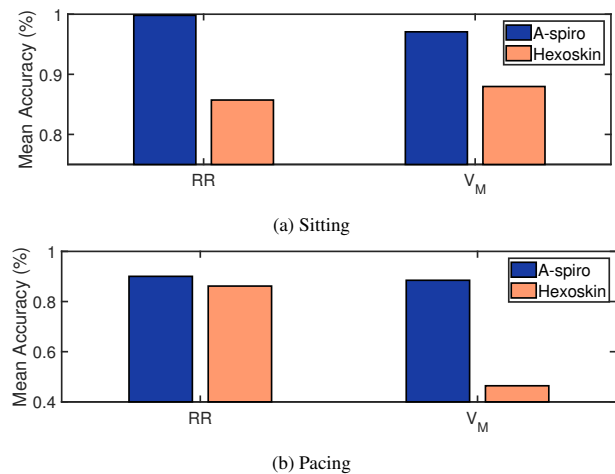


Fig. 19: Relative accuracy in RR , and V_M measurements from A-spiro and Hexoskin against estimations based on flow data from the spirometer using equation 5.

7. Related Work

It has been established that there is a correlation between chest circumference and lung volume as a person inhales and exhales (Shobo & Kakizaki, 2014; Fisher et al., 1990; Sano et al., 2016; Wade, 1954). This correlation has led to a number of different methods for determining respiratory rate and volume indirectly.

Contactless Vital Sign Monitoring. A bulk of recent breathing related work relies on radio frequency for breathing detection. WiSpiro (Nguyen et al., 2016) uses several WiFi emitters mounted on a rail above a patient’s bed to track their respiration rate and minute volume. VitalRadio (Adib et al., 2015) leverages off the shelf WiFi emitters, as do several other works (Liu et al., 2016, 2015; Wang et al., 2017). mmVital (Yang et al., 2017) uses a 60GHz mmWave signal, while DoppleSleep (Rahman et al., 2015) uses radar. VitalRadio, mmVital, and DoppleSleep track the respiration rate of individuals within a home or building, but they do not estimate breathing volume. New methods of photoplethysmography for detecting RR and V_T have also been proposed using a camera (Schoun et al., 2018), as well as a method of using thermal imaging for respiratory monitoring, requiring a patient to blow onto a thin flat material (Patil et al., 2018). Despite their convenience, the main drawback of these contactless sensing techniques is that they require the user to be stationary for the system to perform well. Another limitation is that they are infrastructure dependent, and thus constrained to in-building monitoring, limited to their bed, home, or medical facility. Moreover, these technique are severely impacted by occlusion and human motion. To fill this gap, there has long been an interest in wearable sensors that are able to monitor vital signs continuously without limiting user mobility.

Wearables Systems. There are many methods for measuring expansion and contraction of the chest wall using a sensor band. A common form is the inductance band, which uses a coiled wire embedded in a stretchable fabric that fully encircles the torso. The inductance band allows a precise measurement of the circumference of a user’s chest as they inhale and exhale (Liu et al., 2017, 2013; Fedotov et al., 2017; Wu et al., 2009). It has been evaluated for both RR and V_T with fairly accurate estimations reported for static activities (Cohen et al., 1997; Lanata et al., 2010). Available systems typically track RR , with the exception of the Hexoskin Vest (Villar et al., 2015) which estimates V_M using two sensing units (chest and abdomen) on the vest. Some research, including results presented in this manuscript, indicates the volume estimation is not always reliable (Banerjee et al., 2018; van Leuteren et al., 2017). This is likely due to the added noise of body motion. Another system (Teichmann et al., 2015) uses a sensor that can be placed in a shirt pocket. It also uses inductance, but instead of measuring the stretch of the coil, the sensor measures the interference with an inductive coil caused by changes in impedance in the wearer’s skin. This system does not estimate lung volume

or flow. Similar to Hexoskin, a recent paper suggested a smart shirt that uses a series of 12 fiber optic sensors and reports a bias of 0.9L for V_T estimation (Massaroni et al., 2018).

Mobile Spirometry. Due to the need for spirometry as a tool for diagnosing certain pulmonary diseases (Wolfenden et al., 2006), there have been a number of novel approaches for making spirometry more broadly available. Systems such as TeleSpiro (Carspecken et al., 2013) and MobileSpiro (Gupta et al., 2011) both offer lightweight portable spirometers that can be used with mobile devices. SpiroSmart (Larson et al., 2012), and mCOPD (Xiao, 2013) take it a step further by leveraging the mobile phone itself to measure lung function. The user blows across the microphone of the mobile phone, and the flow rate is calculated based on the sound levels. These approaches require the user to hold something up to their mouth while the test is performed, and is not suitable for continuous monitoring. Due to the nature of the technique, spirometry tests result in a single measurement of a person's health at a single point in time. To remove the need for measuring at the mouth, it is possible to derive the volume or flow indirectly by measuring the chest. This would then allow for a more comfortable sensor placement and continuous monitoring.

8. Discussion

We discuss a few limitations of A-spiro and ideas for potential applications.

Sensor Mounting. Measurements from wearable sensors are affected by body motion and position. While we have addressed the interference cause by body motion, our system is still affected by its mounting. For example, if the sensor is worn loosely, it will generate a large amount of noise.

Non vigorous motion. The current implementation is designed to address daily activities that are non vigorous by nature. It is a feasibility study in accurate estimation of respiratory flow and volume in ambulatory conditions. We have not validated the system for intense or vigorous motion. We believe that the current system can be extended to handle vigorous body movements.

Abdominal motion. A-spiro measures the movement of the chest wall. While our results show that this is suitable for many individuals, users with reduced or impaired chest movement due to open heart surgery (Westerdahl et al., 2003), or other factors, may have inaccurate results. This could be resolved by changing the position of the band to capture abdominal motion associated with lung function.

Energy. To truly allow continuous monitoring, power consumption plays an important role. We have not focused on energy consumption of A-spiro in this paper. However, based on our practical experience, we believe that A-spiro is not likely to be power hungry. We intend to characterize the energy profile of A-spiro in the future. Moreover, with the advancements in battery technology, we anticipate that a wearable system like A-spiro will be able to harvest energy from breathing/body motion.

Future Work. Keeping up with the trend of mobile health (Prasanna et al., 2013), we aim to expand A-spiro to measure other pulmonary measures, such as those involving forced maneuvers. These parameters are critical in measuring lung capacity and are indicative of the existence of serious lung ailments. In a future study, we will recruit participants with breathing disorders for a robust validation of A-spiro. Moreover, A-spiro can be elaborated on to determine the impact of breathing on activities and vice versa. For example, one can monitor their breathing during athletic events, such as weight lifting or playing a sport, to determine their performance and how changes in breathing affect performance. Moreover, real-time fine-grained breathing estimates can provide an insight into psychological experiences, including but not limited to stress and user experience.

9. Conclusion

Human motion has conventionally been looked at as a hindrance to breathing measurement. Even parameters such as breathing rate have been shown to be affected by minor motion, thus limiting continuous breathing monitoring. This paper introduces A-spiro, which breaks away from this assumption and demonstrates that a wearable sensor can be used to accurately measure breathing parameters even during everyday activities, such as transitioning from sitting to standing, lifting-carrying-setting things down, and even walking. We evaluate A-spiro for 20 participants from various ethnicities and age groups to show that it can provide accurate estimates for respiratory rate, tidal flow, and minute ventilation. A-spiro can potentially aid in monitoring breathing for patients with pulmonary disorders, such as COPD and Cystic Fibrosis, specially those that are unable to observe or describe irregular breathing patterns, such as children and older adults with impairments and memory deficiencies. Given the low-cost and untethered nature of the prototype, it can be used to understand the relationship between breathing and body motion at a granular level, particularly useful for athletes and patients with anxiety or aggression.

References

- Abdelnasser, H., Harras, K. A., & Youssef, M. (2015). Ubibreathe: Ubiquitous non-invasive wifi-based breathing estimator. *CoRR, abs/1505.02388*. URL: <http://arxiv.org/abs/1505.02388>. arXiv:1505.02388.
- Adib, F., Mao, H., Kabelac, Z., Katabi, D., & Miller, R. C. (2015). Smart homes that monitor breathing and heart rate. In *Proceedings of the 33rd Annual ACM Conference on Human Factors in Computing Systems CHI '15* (pp. 837–846). New York, NY, USA: ACM. URL: <http://doi.acm.org/10.1145/2702123.2702200>. doi:10.1145/2702123.2702200.
- Banerjee, T., Peterson, M., Oliver, Q., Froehle, A., & Lawhorne, L. (2018). Validating a commercial device for continuous activity measurement in the older adult population for dementia management. *Smart Health, 5-6*, 51 – 62. URL: <http://www.sciencedirect.com/science/article/pii/S2352648317300168>. doi:<https://doi.org/10.1016/j.smhl.2017.11.001>. Wearable Sensor Signal Processing for Smart Health.
- Carspecken, C. W., Arteta, C., & Clifford, G. D. (2013). Telespiro: A low-cost mobile spirometer for resource-limited settings. In *2013 IEEE Point-of-Care Healthcare Technologies (PHT)* (pp. 144–147). doi:10.1109/PHT.2013.6461305.
- Chopra, D. (2018). Tech insider: Deepak chopra's go-to 3-minute meditation to stay focused. URL: <https://youtu.be/4Bs0qUB3BHQ>.
- Cleveland Clinic (2010). Center for Continuing Education:pulmonary function testing. URL: <https://bit.ly/105GTaU>.
- Cohen, K., Ladd, W., Beams, D., Sheers, W., Radwin, R., Tompkins, W., & Webster, J. (1997). Comparison of impedance and inductance ventilation sensors on adults during breathing, motion, and simulated airway obstruction. *IEEE transactions on bio-medical engineering, 44*, 555–566. URL: <https://doi.org/10.1109/10.594896>. doi:10.1109/10.594896.

- Colominas, M. A., Schlotthauer, G., & Torres, M. E. (2014). Improved complete ensemble emd: A suitable tool for biomedical signal processing. *Biomedical Signal Processing and Control*, 14, 19–29. URL: <http://www.sciencedirect.com/science/article/pii/S1746809414000962>. doi:<https://doi.org/10.1016/j.bspc.2014.06.009>.
- El-Tatar, A., & Fokapu, O. (2011). Modeling nr induced artifacts contaminating electrophysiological signals recorded during mri. In *2011 Annual International Conference of the IEEE Engineering in Medicine and Biology Society* (pp. 7135–7138). doi:10.1109/IEMBS.2011.6091803.
- Fang, B., Lane, N. D., Zhang, M., Boran, A., & Kawasar, F. (2016). Bodyscan: Enabling radio-based sensing on wearable devices for contactless activity and vital sign monitoring. In *Proceedings of the 14th Annual International Conference on Mobile Systems, Applications, and Services MobiSys '16* (pp. 97–110). New York, NY, USA: ACM. URL: <http://doi.acm.org/10.1145/2906388.2906411>. doi:10.1145/2906388.2906411.
- Fedotov, A., Akulov, S., & Akulova, A. (2017). Motion artifacts reduction in wearable respiratory monitoring device. (pp. 1121–1124).
- Fisher, L. R., Cawley, M. I., & Holgate, S. T. (1990). Relation between chest expansion, pulmonary function, and exercise tolerance in patients with ankylosing spondylitis. *Annals of the Rheumatic Diseases*, 49, 921–925. URL: <https://www.ncbi.nlm.nih.gov/pmc/articles/PMC1004263/>.
- Gupta, S., Chang, P., Anyigbo, N., & Sabharwal, A. (2011). mobilespiro: Accurate mobile spirometry for self-management of asthma. In *Proceedings of the First ACM Workshop on Mobile Systems, Applications, and Services for Healthcare mHealthSys '11* (pp. 1:1–1:6). New York, NY, USA: ACM. URL: <http://doi.acm.org/10.1145/2064942.2064944>. doi:10.1145/2064942.2064944.
- Huang, N. E., Shen, Z., Long, S. R., Wu, M. C., Shih, H. H., Zheng, Q., Yen, N.-C., Tung, C. C., & Liu, H. H. (1998). The empirical mode decomposition and the hilbert spectrum for nonlinear and non-stationary time series analysis. *Proceedings of the Royal Society of London. Series A: Mathematical, Physical and Engineering Sciences*, 454, 903–995. doi:10.1098/rspa.1998.0193.
- Jones, R., Whittaker, M., Hanney, K., & Shackell, B. (2005). A pilot study of a mobile spirometry service in primary care. *Primary Care Respiratory Journal*, 14, 169–171. URL: <http://dx.doi.org/10.1016/j.pcrj.2004.12.003>. doi:10.1016/j.pcrj.2004.12.003.
- Kumar, S., Nilsen, W. J., Abernethy, A., Atienza, A., Patrick, K., Pavel, M., Riley, W. T., Shar, A., Spring, B., Spruijt-Metz, D., Hedeker, D., Honavar, V., Kravitz, R., Lefebvre, R. C., Mohr, D. C., Murphy, S. A., Quinn, C., Shusterman, V., & Swendeman, D. (2013). Mobile health technology evaluation: The mhealth evidence workshop. *American Journal of Preventive Medicine*, 45, 228–236. URL: <http://www.sciencedirect.com/science/article/pii/S0749379713002778>. doi:<https://doi.org/10.1016/j.amepre.2013.03.017>.
- Lanata, A., Scilingo, E. P., Nardini, E., Loriga, G., Paradiso, R., & De-Rossi, D. (2010). Comparative evaluation of susceptibility to motion artifact in different wearable systems for monitoring respiratory rate. *IEEE Transactions on Information Technology in Biomedicine*, 14, 378–386. doi:10.1109/TITB.2009.2037614.
- Larson, E. C., Goel, M., Boriello, G., Heltshe, S., Rosenfeld, M., & Patel, S. N. (2012). Spirosmart: Using a microphone to measure lung function on a mobile phone. In *Proceedings of the 2012 ACM Conference on Ubiquitous Computing UbiComp '12* (pp. 280–289). New York, NY, USA: ACM. URL: <http://doi.acm.org/10.1145/2370216.2370261>. doi:10.1145/2370216.2370261.
- van Leutenen, R., Fabius, T., de Jongh, F., van der Valk, P., Brusse-Keizer, M., & van der Palen, J. (2017). Detecting dynamic hyperinflation in copd patients using a smart shirt: a pilot study. *European Respiratory Journal*, 50. URL: http://erj.ersjournals.com/content/50/suppl_61/PA2214. doi:10.1183/1393003.congress-2017.PA2214. arXiv:<http://erj.ersjournals.com/content>.
- Liu, H., Guo, S., Zheng, K., PhD, X. G., MA, T. K.-A. P., MS, T. S. P., PhD, K. O. P., & PhD, H. M. P. (2017). Reliability and validity of measuring respiration movement using a wearable strain sensor in healthy subjects. *Physical Therapy Science*, 29, 1543–1547. URL: <https://www.ncbi.nlm.nih.gov/pmc/articles/PMC5599817/>. doi:10.1589/jpts.29.1543. arXiv:<https://www.ncbi.nlm.nih.gov/pmc/articles/PMC5599817/>.
- Liu, J., Wang, Y., Chen, Y., Yang, J., Chen, X., & Cheng, J. (2015). Tracking vital signs during sleep leveraging off-the-shelf wifi. In *Proceedings of the 16th ACM International Symposium on Mobile Ad Hoc Networking and Computing MobiHoc '15* (pp. 267–276). New York, NY, USA: ACM. URL: <http://doi.acm.org/10.1145/2746285.2746303>. doi:10.1145/2746285.2746303.
- Liu, S., Gao, R. X., John, D., Staudenmayer, J., & Freedson, P. (2013). Tissue artifact removal from respiratory signals based on empirical mode decomposition. *Annals of Biomedical Engineering*, 41, 1003–1015. URL: <https://doi.org/10.1007/s10439-013-0742-5>. doi:10.1007/s10439-013-0742-5.
- Liu, X., Cao, J., Tang, S., Wen, J., & Guo, P. (2016). Contactless respiration monitoring via off-the-shelf wifi devices. *IEEE Transactions on Mobile Computing*, 15, 2466–2479. doi:10.1109/TMC.2015.2504935.
- Massaroni, C., Venanzi, C., Silvatti, A. P., Lo Presti, D., Saccomandi, P., Formica, D., Giurazza, F., Caponero, M. A., & Schena, E. (2018). Smart textile for respiratory monitoring and thoraco-abdominal motion pattern evaluation. *Journal of Biophotonics*, 11, e201700263. URL: <https://onlinelibrary.wiley.com/doi/abs/10.1002/jbio.201700263>. doi:10.1002/jbio.201700263. arXiv:<https://onlinelibrary.wiley.com/doi/pdf/10.1002/jbio.201700263>.
- New Diagnostic Design (2018). NDD:easy-on pc spirometer. URL: <https://www.nddmed.com/en-us/product/easy-on-pc.html>.
- Nguyen, P., Zhang, X., Halbower, A., & Vu, T. (2016). Continuous and fine-grained breathing volume monitoring from afar using wireless signals. In *IEEE INFOCOM 2016 - The 35th Annual IEEE International Conference on Computer Communications* (pp. 1–9). doi:10.1109/INFOCOM.2016.7524402.
- NOX Medical (2018). Nox t3 sleep monitor. URL: <https://noxmedical.com/products/nox-t3-sleep-monitor/>.
- Nuffield Foundation (2018). Practical Biology:using a spirometer to investigate human lung function. URL: <https://bit.ly/1TUt865>.
- Parreira, V., Tomich, G., Britto, R., & Sampaio, R. (2005). Assessment of tidal volume and thoracoabdominal motion using volume and flow-oriented incentive spirometers in healthy subjects. *Brazilian Journal of Medical and Biological Research*, 38, 1105–1112. URL: <https://bit.ly/2Hnq0Yy>.
- Patil, O. R., Wang, W., Gao, Y., Xu, W., & Jin, Z. (2018). A low-cost, camera-based continuous ppg monitoring system using laplacian pyramid. *Smart Health*, 9-10, 2–11. URL: <http://www.sciencedirect.com/science/article/pii/S235264831830059X>. doi:<https://doi.org/10.1016/j.smhl.2018.07.024>. CHASE 2018 Special Issue.
- Phillips, M., Beach, J., Cathey, M., Lockert, J., & Satterfield, W. (2017). Reliability and validity of the hexoskin wearable body metrics telemetry shirt. *Journal of Sport and Human Performance*, 5. URL: <https://journals.tdl.org/jhp/index.php/JHP/article/view/108>. doi:10.12922/jshp.v5i2.108.
- Prasanna, P., Jain, S., Bhagat, N., & Madabhushi, A. (2013). Decision support system for detection of diabetic retinopathy using smartphones. In *2013 7th International Conference on Pervasive Computing Technologies for Healthcare and Workshops* (pp. 176–179). doi:10.4108/icst.pervasivehealth.2013.252093.
- Rahman, T., Adams, A. T., Ravichandran, R. V., Zhang, M., Patel, S. N., Kientz, J. A., & Choudhury, T. (2015). Dopplesleep: A contactless nonobtrusive sleep sensing system using short-range doppler radar. In *Proceedings of the 2015 ACM International Joint Conference on Pervasive and Ubiquitous Computing UbiComp '15* (pp. 39–50). New York, NY, USA: ACM. URL: <http://doi.acm.org/10.1145/2750858.2804280>. doi:10.1145/2750858.2804280.
- Sano, Y., Mizutani, K., Zempo, K., & Wakatsuki, N. (2016). Lung volume estimation for thoracic respiration via chest size deviation measurement. In *2016 IEEE 5th Global Conference on Consumer Electronics* (pp. 1–4). doi:10.1109/GCCE.2016.7800500.
- Schoun, B., Transue, S., Halbower, A. C., & Choi, M.-H. (2018). Non-contact tidal volume measurement through thin medium thermal imaging. *Smart Health*, 9-10, 37–49. URL: <http://www.sciencedirect.com/science/article/pii/S2352648318300539>. doi:<https://doi.org/10.1016/j.smhl.2018.07.018>. CHASE 2018 Special Issue.
- Shobo, A., & Kakizaki, F. (2014). Relationship between chest expansion and the change in chest volume. *Rigakuryoho Kagaku*, 29, 881–884. doi:10.1589/rika.29.881.
- Stretch Sense (2017). Stretch sense: Fabric stretch sensor quick start guide + datasheet. URL: <https://bit.ly/2Wnzzx9>.
- Teichmann, D., De Matteis, D., Bartelt, T., Walter, M., & Leonhardt, S. (2015). A bendable and wearable cardiorespiratory monitoring device fusing two noncontact sensor principles. *IEEE Journal of Biomedical and Health Informatics*, 19, 784–793. doi:10.1109/JBHI.2015.2417760.
- Terrien, J., Marque, C., & Karlsson, B. (2011). Automatic detection of mode mixing in empirical mode decomposition using non-stationarity detection: application to selecting imfs of interest and denoising. *EURASIP Journal on Advances in Signal Processing*, 2011, 37. URL: <https://doi.org/10.1186/1687-6180-2011-37>. doi:10.1186/1687-6180-2011-37.
- Villar, R., Beltrame, T., & Hughson, R. L. (2015). Validation of the hexoskin wearable vest during lying, sitting, standing, and walking activities. *Applied Physiology, Nutrition, and Metabolism*, 40, 1019–1024. URL: <https://doi.org/10.1139/apnm-2015-0140>. doi:10.1139/apnm-2015-0140. arXiv:<https://doi.org/10.1139/apnm-2015-0140>. PMID: 26360814.
- Wade, O. L. (1954). Movements of the thoracic cage and diaphragm in respiration*. *The Journal of Physiology*, 124, 193–212. URL: <https://physoc.onlinelibrary.wiley.com/>

- doi:abs/10.1113/jphysiol.1954.sp005099. doi:10.1113/jphysiol.1954.sp005099.
- Wang, X., Yang, C., & Mao, S. (2017). Phasebeat: Exploiting csi phase data for vital sign monitoring with commodity wifi devices. In *2017 IEEE 37th International Conference on Distributed Computing Systems (ICDCS)* (pp. 1230–1239). doi:10.1109/ICDCS.2017.206.
- Westerdahl, E., Lindmark, B., Eriksson, T., Hedenstierna, G., & Tenling, A. (2003). The immediate effects of deep breathing exercises on atelectasis and oxygenation after cardiac surgery. *Scandinavian Cardiovascular Journal*, *37*, 363–367. URL: <https://doi.org/10.1080/14017430310014984>. doi:10.1080/14017430310014984. arXiv:<https://doi.org/10.1080/14017430310014984>. PMID: 14668188.
- Wolfenden, H., Bailey, L., Murphy, K., & Partridge, M. R. (2006). Use of an open access spirometry service by general practitioners. *Primary Care Respiratory Journal*, *15*, 252–255. URL: <http://www.sciencedirect.com/science/article/pii/S1471441806002660>. doi:<https://doi.org/10.1016/j.pcrj.2006.05.007>.
- World Health Organization (2007b). Global surveillance, prevention and control of chronic respiratory diseases. URL: <https://bit.ly/2TnjXW6>.
- World Health Organization (2018a). Chronic respiratory diseases. URL: <http://www.who.int/respiratory/en/#story-03>.
- Wu, D., Wang, L., Zhang, Y. T., Huang, B. Y., Wang, B., Lin, S. J., & Xu, X. W. (2009). A wearable respiration monitoring system based on digital respiratory inductive plethysmography. In *2009 Annual International Conference of the IEEE Engineering in Medicine and Biology Society* (pp. 4844–4847). doi:10.1109/IEMBS.2009.5332665.
- Xiao, L. (2013). *mCOPD: Mobile Phone Based Lung Function Diagnosis and Exercise System for COPD*. Ph.D. thesis. URL: <https://dl.acm.org/citation.cfm?id=2504383> copyright - Database copyright ProQuest LLC; ProQuest does not claim copyright in the individual underlying works; Last updated - 2016-03-11.
- Yang, Z., Pathak, P. H., Zeng, Y., Liran, X., & Mohapatra, P. (2017). Vital sign and sleep monitoring using millimeter wave. *ACM Trans. Sen. Netw.*, *13*, 14:1–14:32. URL: <http://doi.acm.org/10.1145/3051124>. doi:10.1145/3051124.